RSC Sustainability

ROYAL SOCIETY OF CHEMISTRY

PAPER

View Article Online
View Journal | View Issue

Cite this: *RSC Sustainability*, 2024, **2**, 1543

Cellulose nanocrystal-mediated enhancement of hydrogel anti-swelling and water retention

Kudzanai Nyamayaro,[ab] Takeo Iwase,[a] Savvas G. Hatzikiriakos[b] and Parisa Mehrkhodavandi *[a]

Received 13th January 2024
Accepted 14th April 2024

DOI: 10.1039/d4su00016a

rsc.li/rscsus

Research into the creation of flexible electronics has expanded because of the growing interest in wearable electronic devices. The field of iontronics employs ionic conductive hydrogels (IHCs) to access flexible devices that utilize ions as charge carriers. Hydrogel ionic conductors suffer from drawbacks such as low conductivity, water evaporation, over-swelling, and weak mechanical properties. Hydrogels are prone to swelling in aqueous environments; however, excessive swelling is undesirable for water-based applications since overswelling adversely affects the mechanical properties. Here we attempt to improve the anti-swelling and water retention of polyacrylamide hydrogels and poly(acrylamide-*co*-3-sulfopropyl acrylate) ionic conductive hydrogels by incorporating bio-based cellulose nanocrystals (CNCs). Anti-swelling and water retention were accomplished by introducing hydrogen bonding and by ionic complexation through incorporating different weight percent of CNC and employing CNC with varying counter ions. The use of cellulose nanocrystals in ICHs is a pathway toward designing more sustainable ICHs for electronics.

Sustainability spotlight

Hydrogels are a class of materials with a 3D hydrophilic network that can absorb large amounts of water. These materials are used in a wide array of applications that include, iontronics, tissue engineering, drug delivery, contact lenses and wound dressing. Improvement of the mechanical properties of hydrogels expands the potential applications in various fields. Therefore, there is need to develop new sustainable materials to reinforce hydrogels. This work highlights the benefits of using cellulose nanocrystals, a bio-based nanomaterial, to tailor the swelling and water retention properties of hydrogels.

Introduction

Biological systems use ions to conduct signals while devices use electrons. Ionotronics, flexible devices that use both ions and electrons to conduct signals, exist at the interface between biological systems and electronics.[1] Ionotronics made from hybrid circuits have been used in the development of diodes,[2] capacitors,[3] batteries,[2a,b] capacitors,[3] batteries,[4] super capacitors,[5] and transistors.[6]

Ionic conductive hydrogels (ICHs), composed of a liquid phase trapped in a polymer network, can be used in the production of ionotronics.[7] Charged ions may be added to the matrix by using ion-bearing monomers in the polymer network or by dissolving ionic salts in the liquid phase.[8] The practical applicability of ICHs depends on their water content and the microstructure of the hydrogels, which influence their conductivity and mechanical properties.[9] In particular, ionic conductivity is highly influenced by the water content of the hydrogels.[9b] A higher water content increases ionic conductivity by enhancing the mobility and effective diffusion of ions.[10] In parallel, the microstructure of the hydrogel can influence ionic conductivity by allowing ions to migrate more readily in the polymer matrix.[11] Controlling the degree of swelling in ICHs is key to their functionality. Excessive swelling is undesirable for water-based applications since volume expansion due to water absorption adversely affects the mechanical properties of the material.[12] Conversely, ICHs used in non-water based applications can dry out and are prone to losing their functionality over time. Thus, designing ICHs that exhibit anti-swelling for aqueous based applications and water retaining properties under dry conditions is desirable.

Anti-swelling hydrogels can be obtained by weakening polymer–water interactions and strengthening polymer–polymer interactions to reduce osmotic forces within the hydrogel.[13] This has been achieved by employing double network structures, multiple crosslinking, nanocomposites, and supramolecular interactions (hydrogen bonding, hydrophobic association, and ionic complexations).[14] The water retention properties have been improved through a coating or adding hydroscopic matter such as sugars, and glycerol, or through the formation of

[a]*Department of Chemistry, University of British Columbia, Vancouver, BC, Canada. E-mail: mehr@mail.ubc.ca*

[b]*Department of Chemical and Biological Engineering, University of British Columbia, Vancouver, BC, Canada*

nanocomposites with materials like cellulose. Given that both anti-swelling and water retention can be achieved by forming nanocomposites, a hydrogel that exhibits both properties is achievable with the right material.

Herein, we report nanocomposite hydrogels, composed of polyacrylates and cellulose nanocrystals (CNCs), and study their anti-swelling and water retention properties. Firstly, the impact of CNCs with different counter ions (Na, Mg, and Al) on the characteristics of poly(acrylamide) (PAM) is explored. Then, the effect of the CNCs on the characteristics of poly (acrylamide-*co*-3-sulfopropyl acrylate) (poly(AM-*co*-SPA)) ICHs is investigated. The research shows how CNC's intrinsic features may be exploited to affect the anti-swelling and water retention properties of hydrogels systematically. The introduction of biobased nanomaterials in the design of functional materials is a promising strategy towards sustainable products. Despite the use of polyacrylates hydrogels to demonstrate the effectiveness of using CNCs to tailor hydrogel properties, this approach can be applied to degradable hydrogel systems.

Results and discussion

Characterization of CNC-Na, CNC-Mg and CNC-Al

Successful ion exchange was evaluated using zeta potential (ζ), dynamic light scattering (DLS), thermogravimetric analysis (TGA) and Fourier Transform Infrared Spectroscopy (FTIR). Zeta potential is used as a measure of surface charge and colloidal stability of CNCs.[15] The ζ of the CNCs decreased as the valency of the counterion increased (Fig. 1a). The reduction in zeta potential leads to increased interactive forces between CNC particles, allowing the them to aggregate and form a networked structure. The formation of aggregated networks with monovalent, divalent or trivalent ions leads to a relative increase in particle size measured by DLS (Fig. 1b). The effective diameter increases from ~90 nm, which is normal DLS effective diameter for CNC with a Na^+ counterion, to 165 nm with Mg^{2+} and to 1500 nm with Al^{3+} counterions. Thermogravimetric analysis (TGA) data (Fig. 1c) show differences in the thermal properties of CNCs with the different counterions, highlighting that the cation exchange was successful.[16] The FTIR spectra (Fig. 1d) of CNCs with varying counterions display characteristic absorption bands at 3000–3700 cm^{-1} (O–H stretching), ~2900 cm^{-1} (C–H symmetric stretching vibration), 1650 cm^{-1} (absorbed H_2O stretching vibration), and several peaks between 1300–1500 cm^{-1} due to in-plane bending vibration bands of the primary and secondary hydroxy groups.[17]

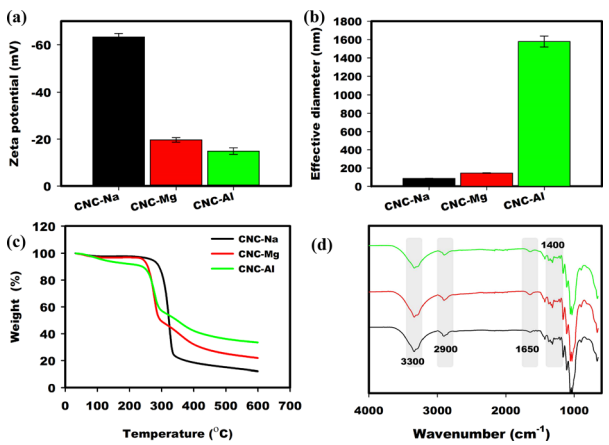

Fig. 1 (a) Zeta potential, (b) dynamic light scattering, (c) thermogravimetric analysis and (d) FTIR of CNC with different counterions.

Design and synthesis of PAM hydrogels

The polyacrylamide (PAM) hydrogels were prepared by free radical polymerization using polyethylene glycol diacrylate (PEGDA) as the crosslinker (Fig. 2). PEGDA was used as a chemical crosslinker because of its hydrophilic nature and biocompatibility, as well as its ability to increase the swelling in a resulting cross-linked hydrogel.[18] We aimed to control the swelling in this highly hydrophilic hydrogel by incorporating cellulose nanocrystals with varying counter ions to increase the overall cross-linking density. The composition of the PAM hydrogel and the different CNC composites are summarized in Table 1.

The hydrogel of pure PAM (**1**) and its composites with 5% CNC-Na (**1A**-5%), CNC-Mg (**1B**-5%) and CNC-Al (**1C**-5%) were dried and analyzed by FTIR spectroscopy (Fig. 3). Cellulose nanocrystals display typical absorption bands at 3000–3700 cm^{-1} (O–H stretching), 2900 cm^{-1} (C–H symmetric stretching vibration), 1642 cm^{-1} (absorbed H_2O stretching vibration), and several peaks between 1300–1500 cm^{-1} due to in-plane bending vibration bands of the primary and secondary hydroxy groups.[17] The spectrum of **1** has characteristic peaks of PAM at 3192 cm^{-1}, 1662 cm^{-1} and 1606 cm^{-1} due to the N–H stretching vibration, C=O stretching vibration and N–H bending vibration of the $-CO-NH_2$ groups, respectively.[19] The spectra of the composites exhibit characteristic features of both cellulose and PAM. In addition, no new absorption peaks are observed, which suggest no chemical reaction between CNC and PAM.[19a,20] Moreover, the adsorption peak at 3436 cm^{-1} for cellulose has shifted to 3404 cm^{-1} and broadened, possibly

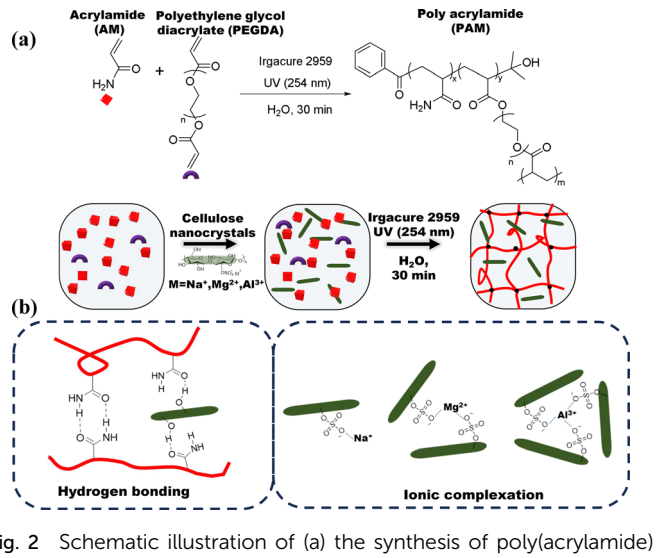

Fig. 2 Schematic illustration of (a) the synthesis of poly(acrylamide) hydrogels and their composite with cellulose nanocrystals with varying counter ions, (b) proposed hydrogen bonding and ionic complexation.

Table 1 Composition of poly(acrylamide) hydrogels and their composite with cellulose nanocrystals with varying counter ions[a]

	Sample	Composition	AM (mol%)	PEGDA (mol%)	CNC (wt%)
1	**1**	PAM_{100}	100	0.05	0
2	**1A**-0.5%	PAM_{100}–0.5% CNC-Na	100	0.05	0.5
3	**1A**-3%	PAM_{100}–3% CNC-Na	100	0.05	3.0
4	**1A**-5%	PAM_{100}–5% CNC-Na	100	0.05	5.0
5	**1B**-0.5%	PAM_{100}–0.5% CNC-Mg	100	0.05	0.5
6	**1B**-3%	PAM_{100}–3% CNC-Mg	100	0.05	3.0
7	**1B**-5%	PAM_{100}–5% CNC-Mg	100	0.05	5.0
8	**1C**-0.5%	PAM_{100}–0.5% CNC-Mg	100	0.05	0.5
9	**1C**-3%	PAM_{100}–3% CNC-Mg	100	0.05	3.0
10	**1C**-5%	PAM_{100}–5% CNC-Mg	100	0.05	5.0

[a] AM-acrylamide, PAM-poly acrylamide, PEGDA-polyethylene glycol diacrylate, CNC-cellulose nanocrystals.

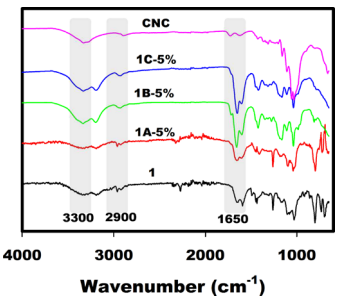

Fig. 3 FTIR spectra of PAM (**1**) and its composites with CNC-Na (**1A**-5%), CNC-Mg (**1B**-5%) and CNC-Al (**1C**-5%).

owing to the formation of hydrogen bonds between cellulose and polyacrylamide chains in the PAM–CNC composites.[21]

Swelling in PAM/CNC-Na composite hydrogels

Equilibrium swelling ratios (ESRs) of **1** and its composite hydrogels with 0.5, 3 and 5 wt% of CNC-Na (**1A**) were measured to investigate their swelling capacity (Fig. 4a). The equilibrium swelling ratio for **1** is 42 g g^{-1} which is in the range of reported ESRs for acrylamide hydrogels (~50 g g^{-1}).[22] CNC-Na (**1A**) composites exhibit lower swelling ratios with increasing amount of CNC-Na : ESRs at 0.5 and 3 wt% lowered to 32 g g^{-1} and 30 g g^{-1} respectively (Fig. 4a). The incorporation of CNC-Na into PAM decreases its swelling capacity, likely due to an increase in the hydrogen bond crosslinking density in the hydrogel network. In addition, the CNCs act as fillers in the matrix of the hydrogel which reduces its porosity.[21] However, when the CNC-Na loading was increased to 5 wt%, the ESR increased (Fig. 3a). This phenomenon was reported for high loadings of CNC and has been attributed to the interference of large amounts of CNCs on chemical crosslinking during polymerization, leading to a decrease in crosslink density.[20] Similar results were observed when CNC-Mg and CNC-Al were used. The equilibrium swelling ratios of **1** with CNC-Mg (**1B**) and CNC-Al (**1C**) were lower at 0.5 and 3 wt% loading, whereas at 5 wt% the ESR increased (Fig. 4b and c).

Water retention of PAM/CNC composite hydrogels

To preserve functionality, ICHs should retain water for as long as possible. Water retention can be quantified as the length of time that the hydrogels can preserve their water content.

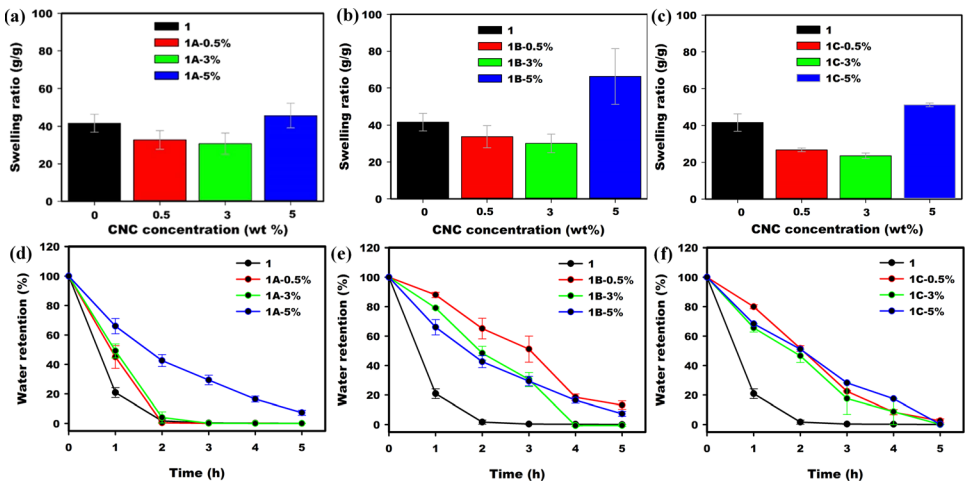

Fig. 4 Equilibrium swelling ratios of PAM (**1**) and its composites with (a) CNC-Na (**1A**), (b) CNC-Mg (**1B**) and (c) CNC-Al (**1C**). Water retention of PAM (**1**) and its composites with (d) CNC-Na (**1A**), (e) CNC-Mg (**1B**) and (f) CNC-Al (**1C**).

Cellulose can lower the rate of water evaporation due to the presence of hydrogen bonding hydroxyl groups on the surface. As shown in Fig. 4d, at 80 °C hydrogel **1** retained 20% of its water weight after 1 h, while CNC-Na (**1A**) at loadings of 0.5, 3, and 5 wt% retained 50, 50, and 70% of their water weight under these conditions. At 5 wt% of **1A**, the water retention capacity extends to 20% after 4 h under these conditions. This increased water retention can be attributed to increased hydrogen bonding due to the hydroxyl groups of CNC.[21,23]

The increase in water retention is enhanced when higher valent salts of CNC are used. For composites CNC-Mg (**1B**) (Fig. 4e) and CNC-Al (**1C**) (Fig. 4d) the water retention improved at all loadings of CNC. After 1 h, hydrogel **1** retained 20% of its water weight, while CNC-Mg (**1B**) and CNC-Al (**1C**) at loadings of 0.5, 3, and 5 wt% retained more than 60% of their water weight. A portion of this increase can be attributed to the increasing hydration number which in turn increases with valency.[24] However, given the very small concentration of counter ions introduced with the CNC, other factors, such as a change in the porosity of the hydrogels due to different connectivity from the different valence counter ions, may have a higher impact on water retention.

Morphological analysis of PAM/CNC composite hydrogels

Fig. 5 depicts the SEM micrographs of PAM composites with 3% CNC-Na (**1A**-3%), CNC-Mg (**1B**-3%) and CNC-Al (**1C**-3%) hydrogels that were swollen in water for 24 h. The presence of CNCs in PAM hydrogel composites has been shown to result in of three-dimensional pore structure.[25] Similarly, a network structure was observed in the PAM/CNC-Na composite, with the pores clearly visible in the 100 μm length scale. Conversely, PAM/CNC-Mg and PAM/CNC-Al do not have an observable pore structure at the same 100 μm length scale. However, when imaged at 20 μm length scale the pores in the PAM/CNC-Mg and PAM/CNC-Al hydrogels are visible. Thus, the increased crosslinking going from CNC-Na to CNC-Mg and CNC-Al resulted in smaller pores and visibly different network structure.

Design and synthesis of poly(AM-*co*-SPA) hydrogels and composites

In the previous sections, it was demonstrated that for an uncharged hydrogel like PAM (**1**), the incorporation of CNCs with varying counter ions imparts the hydrogel with anti-swelling behavior and enhanced water retention properties. In this section, the aim is to apply the same strategy in a hydrogel containing acrylamide (AM) and charged monomer 3-sulfopropyl acrylate (SPA) and investigate whether the properties of the ICH can be tuned in the same manner. The synthesis of poly(AM-*co*-SPA) hydrogels and composites with CNC with varying counter ions is illustrated in Fig. 6. Due to the presence of charged monomers in the solution, the CNC particles aggregate; this is typical behavior when CNCs are in the presence of salts.[26] To counter this effect, the solution was sonicated to obtain a well dispersed colloidal system. The polymerization initiator was added immediately following sonication to avoid reaggregation of the CNCs. The composition of the poly (AM-*co*-SPA) hydrogels and the different CNC composites are summarized in Table 2.

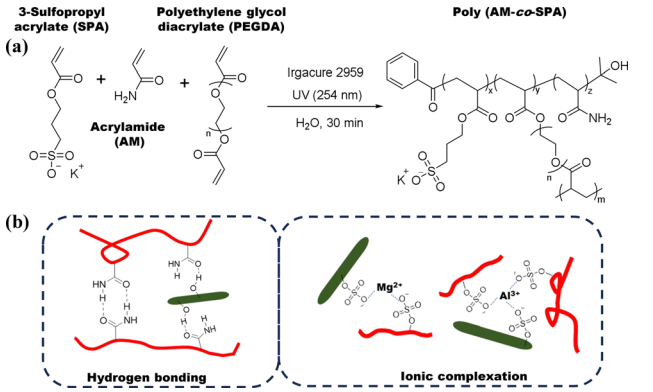

Fig. 6 (a) Synthesis of poly(AM-*co*-SPA) hydrogels and their composite with cellulose nanocrystals with varying counter ions, and (b) proposed hydrogen bonding and ionic complexation.

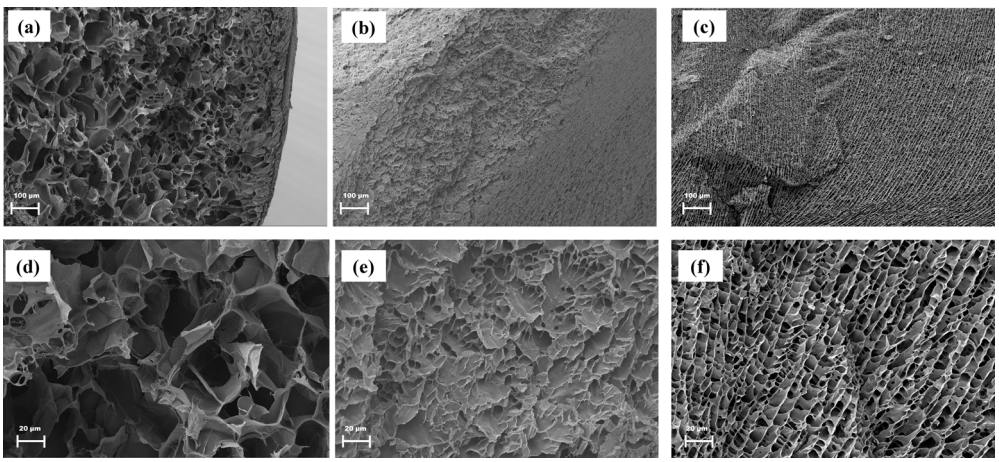

Fig. 5 SEM micrographs of with (a) PAM/CNC-Na (**1A**), (b) PAM/CNC-Mg (**1B**) and (c) PAM/CNC-Al (**1C**). At 100× magnification and (d) PAM/CNC-Na (**1A**), (e) PAM/CNC-Mg (**1B**) and (f) PAM/CNC-Al (**1C**) at 500× magnification.

Table 2 Composition of poly (AM-*co*-SPA) hydrogels and their composite with cellulose nanocrystals with varying counter ion

	Sample	Composition	AM[a] (%)	SPA[a] (%)	PEGDA[a] (%)	CNC[a] (%)
1	**2**	$P(AM_{95}–SPA_5)$	95	5	0.05	0
2	**2A**-0.5%	$P(AM_{95}–SPA_5)$–0.5% CNC-Na	95	5	0.05	0.5
3	**2A**-3%	$P(AM_{95}–SPA_5)$–3% CNC-Na	95	5	0.05	3
4	**2A**-5%	$P(AM_{95}–SPA_5)$–5% CNC-Na	95	5	0.05	5
5	**2B**-0.5%	$P(AM_{95}–SPA_5)$–0.5% CNC-Mg	95	5	0.05	0.5
6	**2B**-3%	$P(AM_{95}–SPA_5)$–3% CNC-Mg	95	5	0.05	3
7	**2B**-5%	$P(AM_{95}–SPA_5)$–5% CNC-Mg	95	5	0.05	5
8	**2C**-0.5%	$P(AM_{95}–SPA_5)$–0.5% CNC-Mg	95	5	0.05	0.5
9	**2C**-3%	$P(AM_{95}–SPA_5)$–3% CNC-Mg	95	5	0.05	3
10	**2C**-5%	$P(AM_{95}–SPA_5)$–5% CNC-Mg	95	5	0.05	5
11	**3**	$P(AM_{80}–SPA_{20})$	80	20	0.05	0
12	**3A**-0.5%	$P(AM_{80}–SPA_{20})$–0.5% CNC-Na	80	20	0.05	0.5
13	**3A**-3%	$P(AM_{80}–SPA_{20})$–3% CNC-Na	80	20	0.05	3
14	**3A**-5%	$P(AM_{80}–SPA_{20})$–5% CNC-Na	80	20	0.05	5
15	**3B**-0.5%	$P(AM_{80}–SPA_{20})$–0.5% CNC-Mg	80	20	0.05	0.5
16	**3B**-3%	$P(AM_{80}–SPA_{20})$–3% CNC-Mg	80	20	0.05	3
17	**3B**-5%	$P(AM_{80}–SPA_{20})$–5% CNC-Mg	80	20	0.05	5
18	**3C**-0.5%	$P(AM_{80}–SPA_{20})$–0.5% CNC-Mg	80	20	0.05	0.5
19	**3C**-3%	$P(AM_{80}–SPA_{20})$–3% CNC-Mg	80	20	0.05	3
20	**3C**-5%	$P(AM_{80}–SPA_{20})$–5% CNC-Mg	80	20	0.05	5

[a] AM-acrylamide, PAM-poly acrylamide, SPA-3-sulfopropylacrylate, PEGDA-polyethylene glycol diacrylate, CNC-cellulose nanocrystals.

Swelling of pure poly(AM-*co*-SPA) hydrogels

To exclude the influence of crosslinking density on the structure and swelling ratio of the hydrogels, the mole fraction of the crosslinker was kept constant at 0.05 mol% for all hydrogels. The swelling ratios increase from with the mole fraction of SPA, with PAM (**1**) ≪ $P(AM_{95}–SPA_5)$ (**2**) < $P(AM_{80}–SPA_{20})$ (**3**) (Fig. 7). The water uptake of a hydrogel is dependent on the hydrophilicity of the monomer, hydrophilicity of the crosslinker and the degree of crosslinking of the hydrogel.[27] In particular, the ionic and hydrophilic poly(SPA) has been used as super absorbent hydrogels.[28] Therefore, increasing the fraction of SPA in the copolymer hydrogel results in higher swelling ratios.

Swelling of poly(AM-*co*-SPA)/CNC-Na composite hydrogels

The impact of added CNC-Na to the charged copolymer poly(AM-*co*-SPA) increases with increased fraction of SPA in the polymer, allowing us to tune the swelling properties. While the ESRs of $P(AM_{95}–SPA_5)$ (**2**) and its composite hydrogels with CNC-Na (**2A**) at loadings of 0.5, 3 and 5 wt% are relatively independent of CNC-Na addition (Fig. 8a and Table 2 entries 1–4), when $P(AM_{80}–SPA_{20})$ (**3**) with higher fraction of charged monomer is used, a drastic decrease in ESR is observed (Fig. 8b, entries 11–14). The decrease in swelling ratio was more pronounced due to presence of more charged groups that can participate in interactions with CNC, effectively increasing the crosslinking density.

Swelling of poly(AM-*co*-SPA)/CNC-Mg and poly(AM-*co*-SPA)/CNC-Al composite hydrogels

CNC-Mg and CNC-Al, are more effective at crosslinking the hydrogel network and thus contribute to a drastic decrease in the swelling ratio of poly(AM-*co*-SPA) composite hydrogels (Fig. 9). Comparable trends are observed in the ESR values for both **2** and **3**, highlighting the importance of the CNC counterions, Mg^{2+} and Al^{3+}, in controlling swelling ratios. The presence of multivalent ions results in the formation of ''ionic crosslinks'' with the anionic groups in the polymer network. This explanation is consistent with the results shown in Fig. 9c and d, illustrating that $P(AM_{80}–SPA_{20})$ (**3**) hydrogel samples which contained a greater concentration of SPA were more sensitive to the presence of multi-valent ions, displaying greater reductions in swelling. Similar results have been reported for

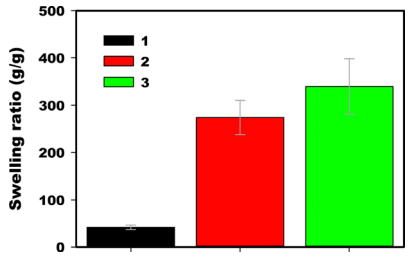

Fig. 7 Equilibrium swelling ratios of PAM (**1**) and poly(AM-*co*-SPA) with different monomer ratios $P(AM_{95}–SPA_5)$ (**2**) and $P(AM_{80}–SPA_{20})$ (**3**).

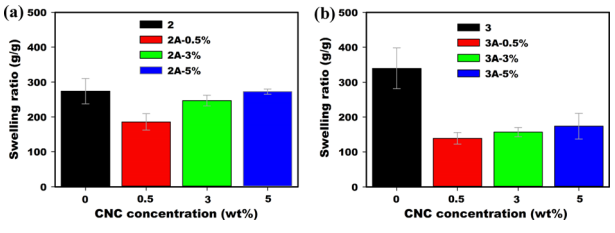

Fig. 8 Equilibrium swelling ratios of (a) $P(AM_{95}–SPA_5)$ (**2**) and its composites with CNC-Na (**2A**) and (b) $P(AM_{80}–SPA_{20})$ (**3**) and its composites with CNC-Na (**3A**).

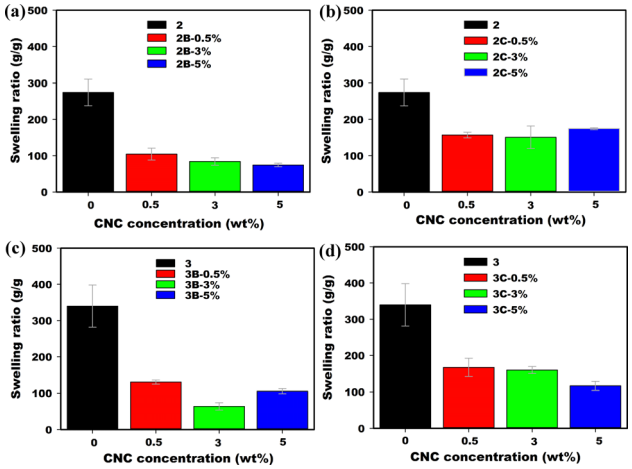

Fig. 9 Equilibrium swelling ratios of P(AM_{95}–SPA_5) (**2**) and its composites with (a) CNC-Mg (**2B**) and (b) CNC-Al (**2C**). Equilibrium swelling ratios of P(AM_{80}–SPA_{20}) (**3**) and its composites with (c) CNC-Mg (**3B**) and (d) CNC-Al (**3C**).

a copolymer of acrylamide and sodium acrylate that were swollen in the presence of salts with varying valency.

Water retention of poly(AM-*co*-SPA) hydrogels

The presence of salts in poly(AM-*co*-SPA) strongly enhances their water retention capability. Addition of further charged CNC's to these polymers does not change their water retention ability in a significant or systematic way, and changes are unpredictable between systems (Fig. 10).

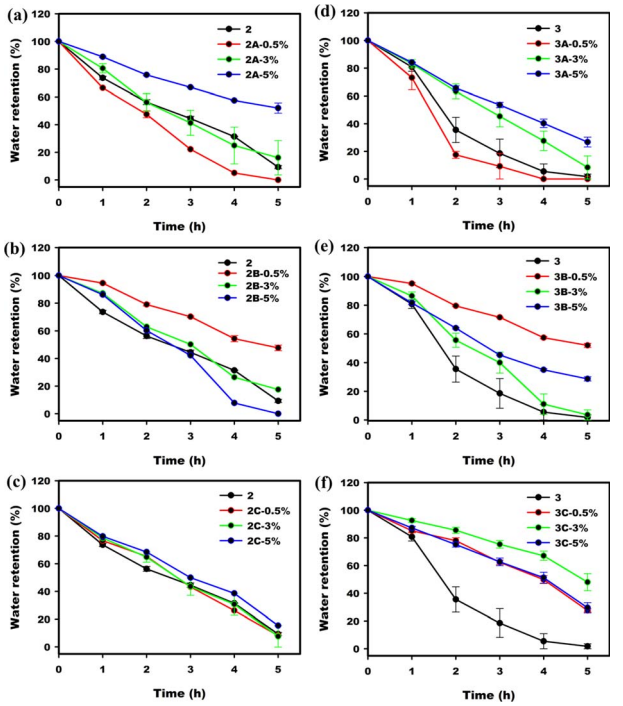

Fig. 10 Water retention of P(AM_{95}–SPA_5) (**2**) and its composites with (a) CNC-Na (**2A**), (b) CNC-Mg (**2B**) and (c) CNC-Al (**2C**). Equilibrium swelling ratios of P(AM_{80}–SPA_{20}) (**3**) and its composites with (d) CNC-Na (**3A**), (e) CNC-Mg (**3B**) and (f) CNC-Al (**3C**).

Conclusions

The goal of this contribution was to design and synthesize nanocomposite hydrogels containing cellulose nanocrystals and study the anti-swelling and water retention properties. A series of poly(acrylamide) and poly(AM-*co*-SPA) nanocomposite hydrogels were successfully designed and fabricated. Cellulose nanocrystals with different valence counter ions were incorporated into the hydrogel matrices by sonication followed by radical polymerization of the acrylate monomers.

Firstly, the anti-swelling and water retention properties of PAM hydrogels were successfully tailored by the incorporation of CNC. Overall, incorporation of cellulose nanocrystals imparted hydrogels with anti-swelling behavior by increasing the crosslinking density and by acting as fillers in the hydrogel matrix. Interestingly, changing from CNC-Na to CNC-Mg and CNC-Al did not influence the extent of anti-swelling. On the other hand, the water retention properties of PAM were significantly changed by moving from CNC-Na to CNC-Mg and CNC-Al. The increased water retention may be attributed to the higher ion hydration number of multivalent ions and the change in network structure of the hydrogels due to the different valence counter ions.

The anti-swelling and water retention properties of poly(AM-*co*-SPA) ionic conducting hydrogels were successfully tuned by the incorporation of CNC. The CNCs with different counter acted as multifunctional crosslinking agents and nanofillers in the ICH network, which significantly reduced the swelling. Highlighting the advantage of employing CNC-Mg and CNC-Al in imparting ICHs with anti-swelling properties. However, the incorporation of CNC into the ICHs did not significantly influence the water retention properties. This was attributed to the presence of larger quantities of ions from 3-sulfopropyl acrylate potassium salt (SPA) which would influence the water retention properties more than the CNC.

Experimental

Materials

Powdered cellulose nanocrystals (CNCs) were obtained from CelluForce (Montreal, QC, Canada) in the form of spray-dried sodium salts with sulfur content of 0.89 wt%, particle size of 1–50 μm (powder), and average hydrodynamic diameter of 70 nm. The following chemicals were purchased from Sigma-Aldrich and used as received without further purification: magnesium hydroxide, and aluminum hydroxide were used in the synthesis of CNCs with varying counter ions; acrylamide (AM) and 3-sulfopropyl acrylate potassium salt (SPA), were used as the monomers; polyethylene glycol diacrylate (PEGDA, M_n = 250 g mol^{-1}) was used as a crosslinker and 2-hydroxy-4′-(2-hydroxyethoxy)-2-methylpropiophenone (Irgacure 2959) was used as the radical initiator.

Synthesis of ion-exchanged charged CNCs

It has been demonstrated that the counterions for sulfonated CNCs can easily be exchanged.[16,29] The commercial sodium

form CNC (Na^+CNC^-) was converted to the acid from (H^+CNC^-) using an ion exchange resin and subsequently neutralized by the corresponding hydroxyl base of the different counterions. In short, a 2 wt% solution of Na^+CNC^- was passed through a Dowex Marathon C hydrogen form ion-exchange resin column. The pH changed from 7 in (Na^+CNC^-) to 3 in H^+CNC^-. The acid form was neutralized by either $Mg(OH)_2$, or $Al(OH)_3$ to produce ($Mg^{2+}(CNC^-)_x$), and ($Al^{3+}(CNC^-)_x$). For simplicity, the notation for the different samples will be CNC followed by the metal cation *i.e.*, CNC-Na, CNC-Mg, and CNC-Al.

Characterization of CNC-Na, CNC-Mg and CNC-Al

Zeta potential (ζ) and dynamic light scattering (DLS) were measured using a NanoBrook Omni (Brookhaven Instruments). Samples were prepared by suspending 0.1 wt% and 0.025 wt% in deionised water for zeta potential and DLS, respectively. The reported results are an average of three independent measurements of each sample. Fourier Transform Infrared Spectroscopy (FTIR) was analysed using a Thermo Scientific Nicolet 6700 FTIR spectrometer. Thermogravimetric analysis (TGA) was carried out on a Netzsch TG 209 F3 Tarsus. 10–20 mg of sample was placed in a ceramic crucible and heated at a rate of 10 °C min^{-1} from 30–600 °C under a nitrogen atmosphere.

Hydrogel preparation

Hydrogels were prepared from 2 M stock solution of the monomers. The molar ratio varied from 100 : 0, 95 : 5 and 80 : 20 AM : SPA to obtain (PAM_{100}), (95AM–5SPA) and (80–20SPA), respectively. Tables 1 and 2 summarize the composition of each hydrogel system. In short, required AM and SPA, Polyethylene glycol diacrylate (PEGDA, $M_n = 250$ g mol^{-1}) were dissolved in 40 mL deionized water. The sample codes for nanocomposite gels containing cellulose are labeled with x% CNC, where the weight concentration of the CNC was against the weight of the water. To make the hydrogel for analysis, the stock solution was first sonicated (3000 J g^{-1}) and stirred vigorously to ensure good dispersion. 2 mL of the stock solution was transferred into a cylindrical glass mold, Irgacure 2959 radical initiator was added, then the solution was deoxygenated by bubbling nitrogen gas for 10 m. Then the resultant solutions were put under UV irradiation for 30 min.

Fourier transform infrared spectroscopy (FTIR)

The structures and interactions in CNC-Na, PAM/CNC-Na, PAM/CNC-Mg, PAM/CNC-Al, and PAM were analysed using a Thermo Scientific Nicolet 6700 FTIR spectrometer in transmission mode. All the spectra were collected from 650 cm^{-1} to 4000 cm^{-1} with a resolution of 4 cm^{-1} and 50 scans.

Scanning electron microscopy (SEM)

SEM was used to investigate the morphological changes of PAM/CNC-Na, PAM/CNC-Mg and PAM/CNC-Al hydrogels. Hydrogels were swollen in distilled water for 24 h then frozen in liquid nitrogen and freeze dried for 48 h. After the lyophilization, the hydrogels were snapped to approximate a cross section and fixed to aluminum SEM stubs using craft glue. The surface was coated with 5 nm AuPd from 3 different angles on a rotary/planetary/tilting stage using a Leica ACE600 sputter coater. The micrographs were obtained using a Zeiss XB350 field emission SEM. Samples were measured at a working distance of 22.9 mm with an accelerating voltage of 5 kV.

Swelling ratio measurement

The gravimetric approach was used to determine the swelling ratio of different hydrogels in distilled water. To achieve equilibrium, the hydrogel samples were swollen in distilled water at room temperature for 48 h. The weight of the swollen hydrogel was measured after the surface water had been dried off using filter paper. Then, the sample was dried in a vacuum oven at 45 °C until the constant weight. The equilibrium swelling ratio (ESR) was calculated as:[20,30]

$$\%\ \mathrm{ESR} = \frac{W_s - W_d}{W_d} \times 100\% \quad (1)$$

where W_s is the weight of the swollen hydrogel and W_d is the weight of the dried gel. Three replicates were performed for each hydrogel and the average value was reported.

Water retention measurement

The deswelling of the hydrogels was measured gravimetrically. First, the hydrogel samples were swollen in distilled water at room temperature for 48 hours. Then, the surface moisture was removed using filter paper and the gel was weighed to obtain W_s. The mass change was measured at 80 °C at regular time intervals. Water retention (WR) is defined as follows:

$$\mathrm{WR} = \frac{W_t - W_d}{W_s - W_d} \times 100\% \quad (2)$$

where W_s and W_d are the weight of water in the swollen gel and weight of dry gel, respectively, and W_t is the weight of the hydrogel at a certain time interval.[31]

Conflicts of interest

There are no conflicts to declare.

Notes and references

1 J. M. Park, S. Lim and J. Y. Sun, *Soft Matter*, 2022, **18**, 6487–6510.
2 (*a*) O. J. Cayre, S. T. Chang and O. D. Velev, *J. Am. Chem. Soc.*, 2007, **129**, 10801–10806; (*b*) K. Nyamayaro, V. Triandafilidi, P. Keyvani, J. Rottler, P. Mehrkhodavandi and S. G. Hatzikiriakos, *Phys. Fluids*, 2021, **33**, 032010; (*c*) K. Nyamayaro, P. Keyvani, F. D'Acierno, J. Poisson, Z. M. Hudson, C. A. Michal, J. D. W. Madden, S. G. Hatzikiriakos and P. Mehrkhodavandi, *ACS Appl. Mater. Interfaces*, 2020, **12**, 52182–52191.
3 P. Janson, E. O. Gabrielsson, K. J. Lee, M. Berggren and D. T. Simon, *Adv. Mater. Technol.*, 2019, **4**, 1800494.

4 A. Manthiram, X. W. Yu and S. F. Wang, *Nat. Rev. Mater.*, 2017, **2**, 16103.
5 M. F. El-Kady, Y. L. Shao and R. B. Kaner, *Nat. Rev. Mater.*, 2016, **1**, 16033.
6 (*a*) H. J. Koo, S. T. Chang and O. D. Velev, *Small*, 2010, **6**, 1393–1397; (*b*) U. J. Kim, S. Kuga, M. Wada, T. Okano and T. Kondo, *Biomacromolecules*, 2000, **1**, 488–492; (*c*) K. Tybrandt, E. O. Gabrielsson and M. Berggren, *J. Am. Chem. Soc.*, 2011, **133**, 10141–10145; (*d*) K. Tybrandt, K. C. Larsson, A. Richter-Dahlfors and M. Berggren, *Proc. Natl. Acad. Sci. U. S. A.*, 2010, **107**, 9929–9932.
7 S. K. De, N. R. Aluru, B. Johnson, W. C. Crone, D. J. Beebe and J. Moore, *J. Microelectromech. Syst.*, 2002, **11**, 544–555.
8 C. H. Yang and Z. G. Suo, *Nat. Rev. Mater.*, 2018, **3**, 125–142.
9 (*a*) W. Wang, R. Narain and H. Zeng, *Front. Chem.*, 2018, **6**, 497; (*b*) C. J. Lee, H. Wu, Y. Hu, M. Young, H. Wang, D. Lynch, F. Xu, H. Cong and G. Cheng, *ACS Appl. Mater. Interfaces*, 2018, **10**, 5845–5852; (*c*) K. Nyamayaro, S. G. Hatzikiriakos and P. Mehrkhodavandi, *RSC Sustainability*, 2023, **1**, 1369–1385; (*d*) Y. Ye, L. Yu, E. Lizundia, Y. Zhu, C. Chen and F. Jiang, *Chem. Rev.*, 2023, **123**, 9204–9264.
10 (*a*) S. De, C. Cramer and M. Schönhoff, *Macromolecules*, 2011, **44**, 8936–8943; (*b*) P. Pissis and A. Kyritsis, *Solid State Ionics*, 1997, **97**, 105–113.
11 (*a*) H. F. Qin, K. Fu, Y. Zhang, Y. H. Ye, M. Y. Song, Y. D. Kuang, S. H. Jang, F. Jiang and L. F. Cui, *Energy Storage Mater.*, 2020, **28**, 293–299; (*b*) J. Hu, Y. Wu, Q. Yang, Q. Zhou, L. Hui, Z. Liu, F. Xu and D. Ding, *Carbohydr. Polym.*, 2022, **275**, 118697; (*c*) H. Wang, Z. Li, M. Zuo, X. Zeng, X. Tang, Y. Sun and L. Lin, *Carbohydr. Polym.*, 2022, **280**, 119018.
12 (*a*) K. I. Hoshino, T. Nakajima, T. Matsuda, T. Sakai and J. P. Gong, *Soft Matter*, 2018, **14**, 9693–9701; (*b*) X. Q. Ming, Y. F. Sheng, L. Yao, X. R. Li, Y. Y. Huang, H. Zhu, Q. Zhang and S. P. Zhu, *Chem. Eng. J.*, 2023, **463**, 142439.
13 (*a*) L. Xu, Z. Huang, Z. Deng, Z. Du, T. L. Sun, Z. H. Guo and K. Yue, *Adv. Mater.*, 2021, **33**, e2105306; (*b*) X. Qi, Q. Zeng, X. Tong, T. Su, L. Xie, K. Yuan, J. Xu and J. Shen, *Hazard. Mater.*, 2021, **402**, 123359.
14 (*a*) Z. B. Wang, H. H. Zhou, D. Liu, X. Chen, D. Wang, S. Dai, F. Chen and B. Xu, *Adv. Funct. Mater.*, 2022, **32**, 2201396; (*b*) X. Di, J. Hou, M. Yang, G. Wu and P. Sun, *Mater. Horiz.*, 2022, **9**, 3057–3069; (*c*) E. K. Feng, J. J. Li, G. C. Zheng, X. Li, J. J. Wei, Z. Q. Wu, X. X. Ma and Z. M. Yang, *Chem. Eng. J.*, 2022, **432**, 134406; (*d*) S. Wang, J. Liu, L. Wang, H. Cai, Q. Wang, W. Wang, J. Shao and X. Dong, *Adv. Mater. Technol.*, 2022, **8**, 2201477.
15 E. J. Foster, R. J. Moon, U. P. Agarwal, M. J. Bortner, J. Bras, S. Camarero-Espinosa, K. J. Chan, M. J. D. Clift, E. D. Cranston, S. J. Eichhorn, D. M. Fox, W. Y. Hamad, L. Heux, B. Jean, M. Korey, W. Nieh, K. J. Ong, M. S. Reid, S. Renneckar, R. Roberts, J. A. Shatkin, J. Simonsen, K. Stinson-Bagby, N. Wanasekara and J. Youngblood, *Chem. Soc. Rev.*, 2018, **47**, 2609–2679.
16 K. Nyamayaro, P. Mehrkhodavandi and S. G. Hatzikiriakos, *Carbohydr. Polym.*, 2023, **302**, 120378.
17 E. J. Foster, R. J. Moon, U. P. Agarwal, M. J. Bortner, J. Bras, S. Camarero-Espinosa, K. J. Chan, M. J. D. Clift, E. D. Cranston, S. J. Eichhorn, D. M. Fox, W. Y. Hamad, L. Heux, B. Jean, M. Korey, W. Nieh, K. J. Ong, M. S. Reid, S. Renneckar, R. Roberts, J. A. Shatkin, J. Simonsen, K. Stinson-Bagby, N. Wanasekara and J. Youngblood, *Chem. Soc. Rev.*, 2018, **47**, 2609–2679.
18 (*a*) J. L. Zhang, N. Wang, W. G. Liu, X. L. Zhao and W. Lu, *Soft Matter*, 2013, **9**, 6331–6337; (*b*) G. C. Ingavle, S. H. Gehrke and M. S. Detamore, *Biomaterials*, 2014, **35**, 3558–3570; (*c*) X. J. Liu, H. Q. Li, B. Y. Zhang, Y. J. Wang, X. Y. Ren, S. Guan and G. H. Gao, *RSC Adv.*, 2016, **6**, 4850–4857.
19 (*a*) Y. Wang, Z. Wang, K. Wu, J. Wu, G. Meng, Z. Liu and X. Guo, *Carbohydr. Polym.*, 2017, **168**, 112–120; (*b*) R. Q. Liu, S. M. Liang, X. Z. Tang, D. Yan, X. F. Li and Z. Z. Yu, *J. Mater. Chem.*, 2012, **22**, 14160–14167.
20 C. Zhou and Q. Wu, *Colloids Surf., B*, 2011, **84**, 155–162.
21 T. Jayaramudu, H. U. Ko, H. C. Kim, J. W. Kim and J. Kim, *Materials*, 2019, **12**, 2080.
22 (*a*) C. Zhou, Q. Wu, Y. Yue and Q. Zhang, *J. Colloid Interface Sci.*, 2011, **353**, 116–123; (*b*) B. G. Li, Y. D. Zhang, Y. F. Han, B. Guo and Z. Y. Luo, *Cellulose*, 2019, **26**, 6701–6711.
23 H. Gharekhani, A. Olad, A. Mirmohseni and A. Bybordi, *Carbohydr. Polym.*, 2017, **168**, 1–13.
24 (*a*) H. Chen and E. Ruckenstein, *J. Phys. Chem. B*, 2015, **119**, 12671–12676; (*b*) H. Ohtaki and T. Radnai, *Chem. Rev.*, 1993, **93**, 1157–1204.
25 F. A. Aouada, M. R. de Moura, W. J. Orts and L. H. C. Mattoso, *J. Agric. Food Chem.*, 2011, **59**, 9433–9442.
26 (*a*) F. Cherhal, F. Cousin and I. Capron, *Langmuir*, 2015, **31**, 5596–5602; (*b*) L. Zhong, S. Fu, X. Peng, H. Zhan and R. Sun, *Carbohydr. Polym.*, 2012, **90**, 644–649; (*c*) T. Phan-Xuan, A. Thuresson, M. Skepö, A. Labrador, R. Bordes and A. Matic, *Cellulose*, 2016, **23**, 3653–3663.
27 Y. Guo, J. Bae, Z. Fang, P. Li, F. Zhao and G. Yu, *Chem. Rev.*, 2020, **120**, 7642–7707.
28 (*a*) S. Scognamillo, V. Alzari, D. Nuvoli, J. Illescas, S. Marceddu and A. Mariani, *J. Polym. Sci., Part A: Polym. Chem.*, 2011, **49**, 1228–1234; (*b*) S. Scognamillo, V. Alzari, D. Nuvoli and A. Mariani, *J. Polym. Sci., Part A: Polym. Chem.*, 2010, **48**, 2486–2490.
29 L. L. Liu, Z. Hu, X. F. Sui, J. Guo, E. D. Cranston and Z. P. Mao, *Ind. Eng. Chem. Res.*, 2018, **57**, 7169–7180.
30 S. Wang, D. H. Kempen, N. K. Simha, J. L. Lewis, A. J. Windebank, M. J. Yaszemski and L. Lu, *Biomacromolecules*, 2008, **9**, 1229–1241.
31 L. Y. Chang, L. J. Xu, Y. H. Liu and D. Qiu, *Polym. Test.*, 2021, **94**, 107021.